

Article

Bifurcated Halogen Bond-Driven Supramolecular Double Helices from 1,2-Dihalotetrafluorobenzene and 2,2'-Bi(1,8-naphthyridine)

Ziyu Wang 

SDU-ANU Joint Science College, Shandong University, Weihai 264209, China; nclab@126.com

Abstract: The unique enantiomeric pairs of double helices have been found in the structure of the cocrystal between 1,2-diiodotetrafluorobenzene and 2,2'-bi(1,8-naphthyridine). The formation of the supramolecular double helices is driven by the strong bifurcated iodine bonds which can force the herringbone packing arrangement of the molecules 2,2'-bi(1,8-naphthyridine) into a face-to-face $\pi\cdots\pi$ stacking pattern. In contrast, the cocrystal between 1,2-dibromotetrafluorobenzene (or 1,2-dichlorotetrafluorobenzene) and 2,2'-bi(1,8-naphthyridine) was not obtained under the same conditions. The interaction energies of the bifurcated halogen bonds and $\pi\cdots\pi$ stacking interactions were computed with the reliable dispersion-corrected density functional theory. The computational results show that the bifurcated iodine bond is much stronger than the bifurcated bromine bond and bifurcated chlorine bond, and it is the much stronger bifurcated iodine bond that makes the cocrystal of 1,2-diiodotetrafluorobenzene and 2,2'-bi(1,8-naphthyridine) much easier to be synthesized.

Keywords: supramolecular double helices; enantiomeric pair; bifurcated halogen bond; $\pi\cdots\pi$ stacking interaction



Citation: Wang, Z. Bifurcated Halogen Bond-Driven Supramolecular Double Helices from 1,2-Dihalotetrafluorobenzene and 2,2'-Bi(1,8-naphthyridine). *Crystals* **2022**, *12*, 937. <https://doi.org/10.3390/cryst12070937>

Academic Editors: Alexander S. Novikov and Longjiu Cheng

Received: 20 June 2022

Accepted: 30 June 2022

Published: 2 July 2022

Publisher's Note: MDPI stays neutral with regard to jurisdictional claims in published maps and institutional affiliations.



Copyright: © 2022 by the author. Licensee MDPI, Basel, Switzerland. This article is an open access article distributed under the terms and conditions of the Creative Commons Attribution (CC BY) license (<https://creativecommons.org/licenses/by/4.0/>).

1. Introduction

Besides the well-known hydrogen bond, the halogen bond and $\pi\cdots\pi$ stacking interaction are the other two important types of noncovalent interactions. In recent years, much of the focus of attention in the field of noncovalent interaction has been on the theoretical and experimental studies of the halogen bond, one of the subsets of the σ -hole bonds [1–13]. The perfluorinated halobenzenes are commonly used halogen atom donors in the crystal engineering involving the halogen bonds. In contrast to the 1,4-dihalotetrafluorobenzene, 1,3-dihalotetrafluorobenzene and 1,3,5-trihalotrifluorobenzene, the 1,2-dihalotetrafluorobenzene is relatively seldom studied because of its two crowded halogen atoms [1–3]. Besides the monocentric halogen bonds, there are also many bifurcated halogen bonds although in most cases the bifurcated halogen bonds are energetically inferior to the monocentric halogen bonds [14]. The bifurcated halogen bonds are frequently seen in the halogen bond-directed cocrystals in which the 1,2-dihalotetrafluorobenzene molecules act as the halogen atom donors [15–18]. There are mainly two kinds of bifurcated halogen bonds: one is the bifurcated halogen bonds with bifurcated halogen atom acceptors [15,16]; the other is the bifurcated halogen bonds with bifurcated halogen atom donors [17,18]. Jin and coworkers reported the structure and optical properties of the cocrystal between 1,2-diiodotetrafluorobenzene and 1,10-phenanthroline driven by the C–I \cdots (N,N) asymmetrical bifurcated halogen bond [18]. The N \cdots N interatomic distance in 1,10-phenanthroline in this cocrystal structure is 2.720 Å. An interesting question is what will happen to the bifurcated halogen bond if the N \cdots N interatomic distance becomes shorter. In this study, we select the 1,2-dichlorotetrafluorobenzene (C₆F₄Cl₂), 1,2-dibromotetrafluorobenzene (C₆F₄Br₂), 1,2-diiodotetrafluorobenzene (C₆F₄I₂) and 2,2'-bi(1,8-naphthyridine) (C₁₆H₁₀N₄) as models to address this question. The molecular structures of C₆F₄Cl₂, C₆F₄Br₂, C₆F₄I₂ and C₁₆H₁₀N₄ are shown in Figure 1. The crystal structure of C₁₆H₁₀N₄ has been reported in 2015 [19].

The distance between two adjacent N atoms in the crystal structure of $C_{16}H_{10}N_4$ is 2.311 Å, which is obviously smaller than the N⋯N interatomic distance in 1,10-phenanthroline. Hence, the molecule $C_{16}H_{10}N_4$ is a very good model for addressing above-mentioned issue.

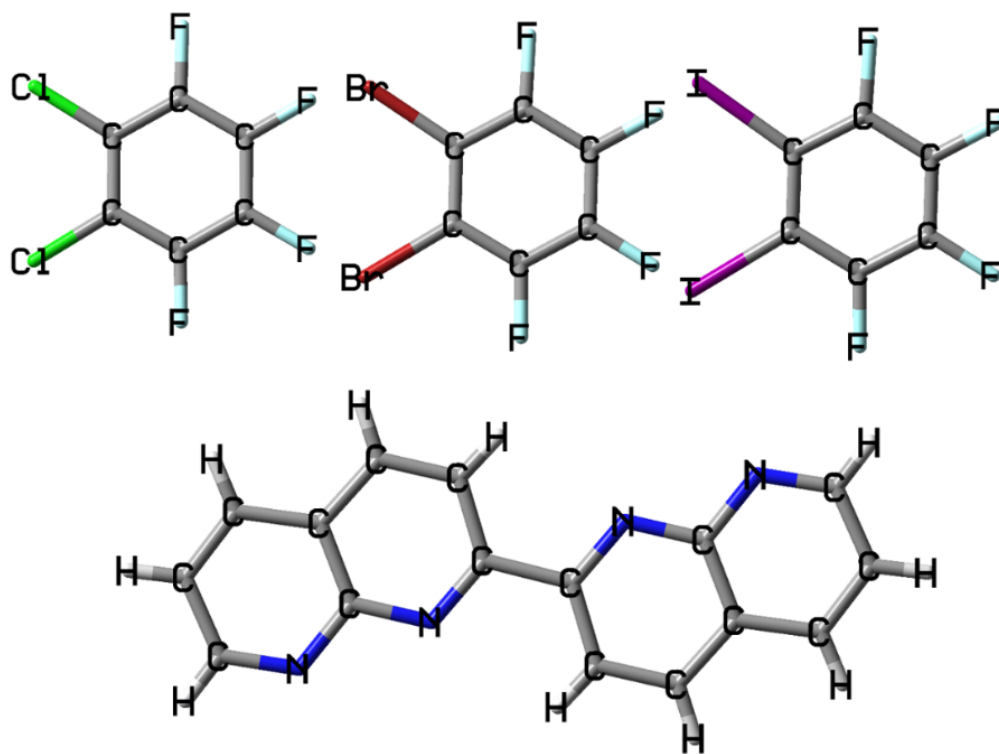


Figure 1. The molecular structures of $C_6F_4Cl_2$, $C_6F_4Br_2$, $C_6F_4I_2$ and $C_{16}H_{10}N_4$.

Figure 2 demonstrates the molecular electrostatic potential maps of $C_6F_4Cl_2$, $C_6F_4Br_2$, $C_6F_4I_2$ and $C_{16}H_{10}N_4$ along with some selected local minima or maxima of the surface electrostatic potentials. The computational details for the molecular electrostatic potentials can be found in Section 2.3. The halogen bond has different subsets such as the chlorine bond, bromine bond and iodine bond [20]. The bifurcated chlorine bond can be formed between $C_6F_4Cl_2$ and $C_{16}H_{10}N_4$; the bifurcated bromine bond can be formed between $C_6F_4Br_2$ and $C_{16}H_{10}N_4$; the bifurcated iodine bond can be formed between $C_6F_4I_2$ and $C_{16}H_{10}N_4$. Theoretically, one $C_{16}H_{10}N_4$ molecule can form two bifurcated halogen bonds with two 1,2-dihalo-2,4,6-trifluorobenzene molecules. As shown in Figure 2, the most positive electrostatic potential on I is larger than that on Br, and the most positive electrostatic potential on Cl is the smallest one. Considering that the strong halogen bond is an electrostatically driven noncovalent interaction [21], it is reasonable to assume the halogen bond strength order of bifurcated iodine bond > bifurcated bromine bond > bifurcated chlorine bond. However, such a strength order may be affected by the $\pi\cdots\pi$ stacking interactions between the halogen atom acceptors $C_{16}H_{10}N_4$. $C_{16}H_{10}N_4$ is a relatively large aromatic molecule. The $\pi\cdots\pi$ stacking interactions between the aromatic molecules $C_{16}H_{10}N_4$ should be strong enough to compete with the bifurcated halogen bonds. The second purpose of this study is thus to explore the strengths of the bifurcated halogen bonds and $\pi\cdots\pi$ stacking interactions and their mutual effects.

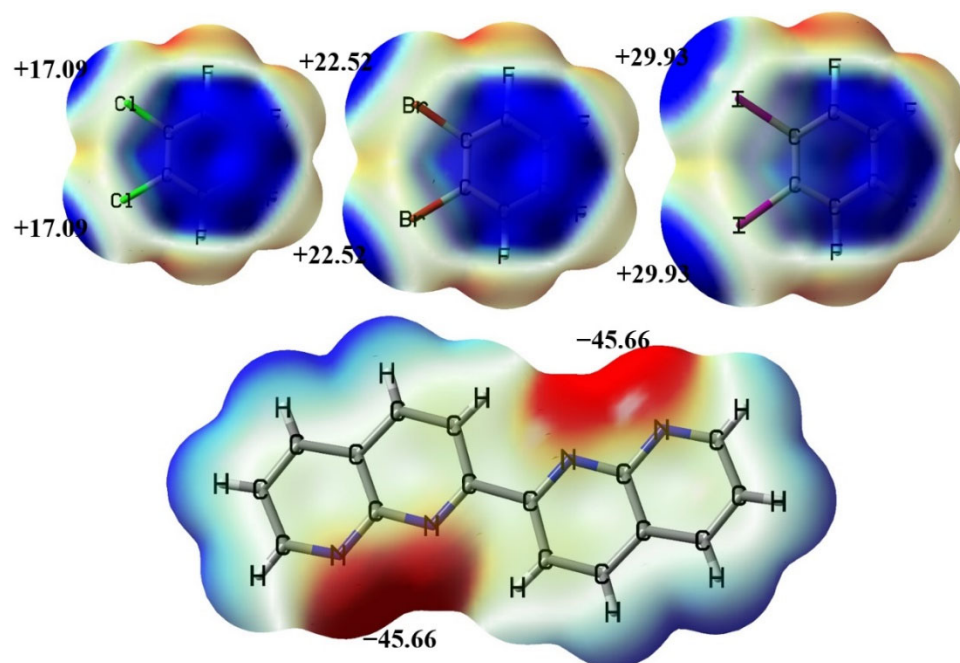


Figure 2. The electrostatic potential maps of the molecules $C_6F_4Cl_2$, $C_6F_4Br_2$, $C_6F_4I_2$ and $C_{16}H_{10}N_4$. The numbers are the local minima or maxima of the surface electrostatic potentials (in kcal/mol).

2. Materials and Methods

2.1. Cocystal Synthesis

The reactants $C_6F_4Br_2$ (liquid, purity $\geq 98\%$), $C_6F_4I_2$ (solid, 98%) and $C_{16}H_{10}N_4$ (solid, purity $\geq 98\%$) were purchased from J&K Scientific Ltd., Beijing, China and $C_6F_4Cl_2$ (liquid, purity $\geq 98\%$) was purchased from Alfa Chemical Co., Ltd., Zhengzhou, China. The solvent chloroform (analytical grade) was obtained commercially from local company in Zhengzhou, China. All the chemicals and solvent were used as received.

A series of binary mixtures of $C_{16}H_{10}N_4$ with $C_6F_4Cl_2$, $C_6F_4Br_2$, and $C_6F_4I_2$, respectively, in different molar ratios (2:1, 1:1 and 1:2) were dissolved in chloroform in glass vials. Each vial was sealed with parafilm having several pinholes for slow solvent evaporation. After the nine glass vials were kept at room temperature for about five days, the colorless single crystals suitable for X-ray diffraction analyses were obtained. However, the X-ray crystal structure resolution performed on these single crystals showed that only the 1:1 cocystal between $C_6F_4I_2$ and $C_{16}H_{10}N_4$ was successfully synthesized, and all the other single crystals are the crystals of $C_{16}H_{10}N_4$. The desirable cocystals between $C_6F_4Cl_2$ and $C_{16}H_{10}N_4$ and between $C_6F_4Br_2$ and $C_{16}H_{10}N_4$ were not obtained.

2.2. X-ray Crystallography

The crystallographic data of the cocystal between $C_6F_4I_2$ and $C_{16}H_{10}N_4$ were collected on the Rigaku Oxford SuperNova diffractometer (Rigaku, Tokyo, Japan) with the Mo-K α radiation ($\lambda = 0.71073 \text{ \AA}$) at a temperature of 289 K. The CrysAlisPro software was used for data processing [22]. The cocystal structure was solved and refined by using the SHELX-2014 and Olex2.0 programs [23–25]. The crystallographic data of the cocystal between $C_6F_4I_2$ and $C_{16}H_{10}N_4$ have been deposited in the Cambridge Crystallographic Data Centre (CCDC), and the deposition number is CCDC 2168308. At the same time, the crystallographic information file of the cocystal between $C_6F_4I_2$ and $C_{16}H_{10}N_4$ was also provided as the Supplementary Material.

2.3. Computational Details

The geometries of the monomers $C_6F_4Cl_2$, $C_6F_4Br_2$, $C_6F_4I_2$ and $C_{16}H_{10}N_4$ were fully optimized at the PBE0-D3(BJ)/def2-TZVPP theory level [26–29]. The PBE0-D3(BJ)/def2-

TZVPP electrostatic potentials of these monomers were calculated on the outer 0.001 a.u. contours of the molecules' electronic densities [21]. Unless otherwise stated, the geometries of the dimers in the crystal structure were not optimized and are extracted directly from the crystal structure. The geometries of the trimers in the gas phase were fully optimized at the PBE0-D3(BJ)/def2-TZVPP level of theory. The PBE0-D3(BJ)/def2-TZVPP interaction energies of the dimers and trimers were calculated using the supermolecule method and the basis set superposition error corrections to the interaction energies were carried out with the counterpoise method [30]. Previous studies have proved that PBE0-D3 is an excellent functional for the study of π -stacked complexes [31,32]. All the calculations were performed with the GAUSSIAN 09 suite of programs [33].

3. Results and Discussion

3.1. The Cocrystal Structure

Figure 3 shows the $2 \times 2 \times 2$ unit cell of the 1:1 cocrystal between $C_6F_4I_2$ and $C_{16}H_{10}N_4$ viewed along the *a* axis. It can be clearly seen from Figure 3 that there exist the bifurcated iodine bonds between $C_6F_4I_2$ and $C_{16}H_{10}N_4$, $\pi \cdots \pi$ stacking interactions between molecules $C_6F_4I_2$ and $\pi \cdots \pi$ stacking interactions between molecules $C_{16}H_{10}N_4$ in the cocrystal structure. For clarity, the weak C–H \cdots F hydrogen bonds in the cocrystal structure are not shown in Figure 3. There are two different C–I \cdots (N,N) bifurcated iodine bonds in the cocrystal structure, and both of them are asymmetrical. The I \cdots N interatomic distances are 2.952(3) and 3.485(2) Å in one C–I \cdots (N,N) bifurcated iodine bond, and are 3.102(4) and 3.473(3) Å in the other C–I \cdots (N,N) bifurcated iodine bond. Firstly, the 2D structure is formed via the bifurcated iodine bonds between $C_6F_4I_2$ and $C_{16}H_{10}N_4$, $\pi \cdots \pi$ stacking interactions between molecules $C_6F_4I_2$ and $\pi \cdots \pi$ stacking interactions between molecules $C_{16}H_{10}N_4$. Then, different 2D structures are connected together by the weak C–H \cdots F hydrogen bonds to form the 3D structure of the cocrystal. The crystallographic data for the cocrystal ($M = 660.14$ g/mol) are summarized as follows: triclinic, space group $P\bar{1}$ (no. 2), $a = 7.3663(3)$ Å, $b = 11.9334(7)$ Å, $c = 13.3466(6)$ Å, $\alpha = 68.924(5)^\circ$, $\beta = 84.768(4)^\circ$, $\gamma = 85.522(4)^\circ$, $V = 1088.89(10)$ Å³, $Z = 2$, $T = 289$ K, $\mu(\text{CuK}\alpha) = 2.939$ mm^{−1}, $D_{\text{calc}} = 2.013$ g/cm³, 15893 reflections measured ($6.508^\circ \leq 2\Theta \leq 56.856^\circ$), 4720 unique ($R_{\text{int}} = 0.0499$, $R_{\text{sigma}} = 0.0489$), which were used in all calculations. The final R_1 was 0.0355 ($I > 2\sigma(I)$) and wR_2 was 0.0846 (all data).

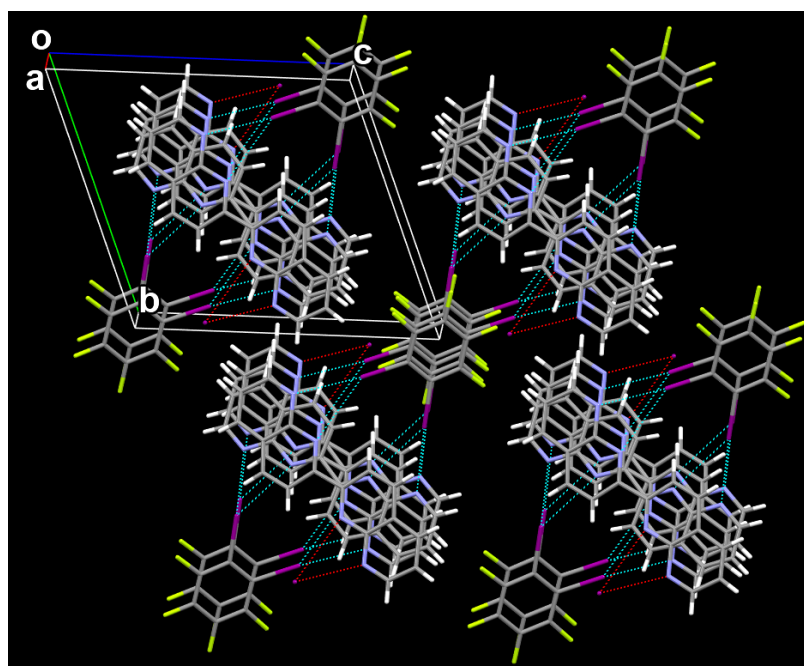


Figure 3. The $2 \times 2 \times 2$ unit cell of the cocrystal viewed along the *a* axis.

Close inspection of the cocrystal structure reveals that a pair of enantiomeric (*P* and *M*) supramolecular double helices are assembled by the bifurcated iodine bonds between $C_6F_4I_2$ and $C_{16}H_{10}N_4$ and $\pi\cdots\pi$ stacking interactions between molecules $C_{16}H_{10}N_4$. Different pairs of *P* and *M* supramolecular double helices are assembled together by the $\pi\cdots\pi$ stacking interactions between molecules $C_6F_4I_2$ to form the 2D structure of the cocrystal. In fact, in recent years the halogen bond-driven supramolecular double helices have been reported in many studies [34–38]. In this work, the *P* supramolecular helix and *M* supramolecular helix share the same π -stacked $C_{16}H_{10}N_4$ molecules to assemble the enantiomeric pair of double helices. This case is very similar to the supramolecular double helices assembled by the hydrogen-bonded 3-mer arylamide foldamer and 1,4-diiidotetrafluorobenzene, in which the *P* supramolecular helix and *M* supramolecular helix also have the overlapping region [36].

The PBE0-D3(BJ)/def2-TZVPP interaction energies of the bifurcated iodine bonds and $\pi\cdots\pi$ stacking interactions can be seen in Figure 4. The interaction energy of the $\pi\cdots\pi$ stacking interaction between two $C_{16}H_{10}N_4$ molecules is -16.47 kcal/mol. In contrast, the interaction energy of the parallel-displaced benzene dimer is only -2.70 kcal/mol [39]. This means that the $\pi\cdots\pi$ stacking interaction between two $C_{16}H_{10}N_4$ molecules is rather strong. There are two different $\pi\cdots\pi$ stacking interactions between $C_6F_4I_2$ molecules, the interaction energies of which are -7.16 and -7.37 kcal/mol, respectively. There are also two different bifurcated iodine bonds in the cocrystal structure, the interaction energies of which are -10.09 and -10.67 kcal/mol, respectively. The PBE0-D3(BJ)/def2-TZVPP interaction energy of the bifurcated iodine bond in the cocrystal between 1,2-diiidotetrafluorobenzene and 1,10-phenanthroline is -9.91 kcal/mol [18]. The interaction energy difference between the bifurcated iodine bonds in the two different cocrystals is very small, which indicates that the strength of the C–I \cdots (N,N) bifurcated iodine bond is not dependent on the N \cdots N interatomic distance. It is well-known that the H atom positions cannot be precisely determined by the single-crystal X-ray diffraction. For the dimers between $C_6F_4I_2$ and $C_{16}H_{10}N_4$ (see Figure 4), we evaluated their interaction energies with and without the optimizations of the H atom positions, and found that the differences are negligible. On the other hand, such a result also reflects that the C–H \cdots I interactions in these dimers are very weak. Throughout this study, we did not discuss the effects of adjacent C–H \cdots I interactions on the bifurcated iodine bonds.

The crystal structure of $C_{16}H_{10}N_4$ can be viewed and retrieved from the Cambridge Structural Database (refcode: QETZIB) [40]. Figure 5 demonstrates different stacking patterns of the two $C_{16}H_{10}N_4$ molecules in the $C_{16}H_{10}N_4$ crystal and in the cocrystal between $C_6F_4I_2$ and $C_{16}H_{10}N_4$. In the π -stacked $C_{16}H_{10}N_4$ dimer in the $C_{16}H_{10}N_4$ crystal, the N atoms of the two $C_{16}H_{10}N_4$ molecules are in the eclipsed arrangement, whereas in the π -stacked $C_{16}H_{10}N_4$ dimer in the cocrystal between $C_6F_4I_2$ and $C_{16}H_{10}N_4$, the N atoms of the two $C_{16}H_{10}N_4$ molecules are in the opposed arrangement. The interaction energy of the former dimer is -11.22 kcal/mol, and the interaction energy of the latter dimer is -16.47 kcal/mol. Although the $\pi\cdots\pi$ stacking interaction of the $C_{16}H_{10}N_4$ dimer in Figure 5b is much stronger than the $\pi\cdots\pi$ stacking interaction of the $C_{16}H_{10}N_4$ dimer in Figure 5a, there is no $C_{16}H_{10}N_4$ dimer in Figure 5b found in the crystal structure of $C_{16}H_{10}N_4$. In the crystal structure of $C_{16}H_{10}N_4$, the $C_{16}H_{10}N_4$ molecules are assembled in a herringbone pattern which is more stable because of the dense packing [41]. That is to say, the 1D columnar stacking structure of the $C_{16}H_{10}N_4$ molecules in the cocrystal between $C_6F_4I_2$ and $C_{16}H_{10}N_4$ is unfavorable in enthalpic gain for the cocrystal formation. However, the introduction of the strong bifurcated iodine bonds offsets the enthalpic loss and promotes the cocrystal formation. It can be concluded here that the bifurcated iodine bond changes the stacking pattern of the $C_{16}H_{10}N_4$ molecules and the cocrystal formation is driven by the bifurcated iodine bond.

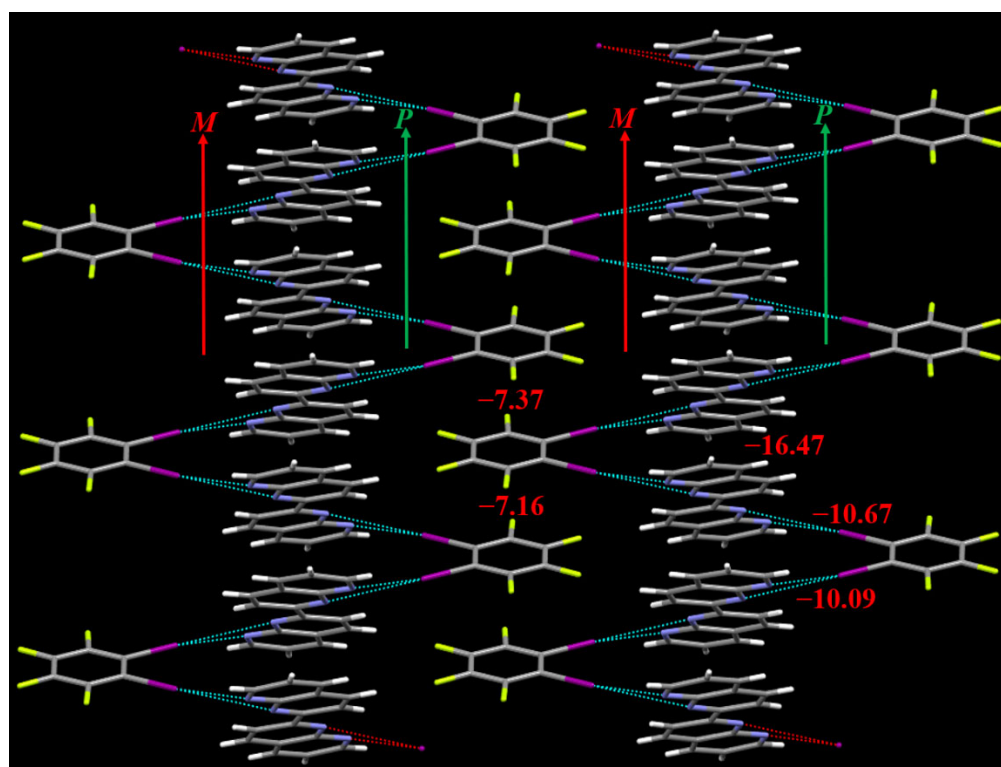


Figure 4. The enantiomeric pair of double helices in the cocrystal structure. The red numbers are the interaction energies (kcal/mol) of the bifurcated iodine bonds and $\pi\cdots\pi$ stacking interactions.

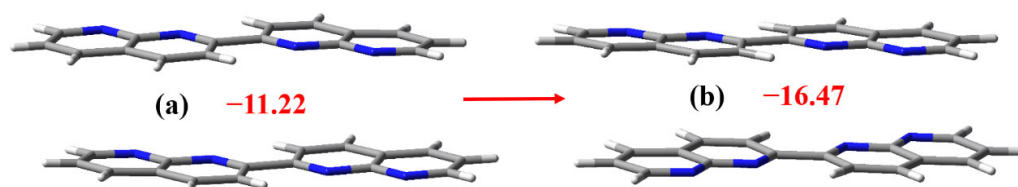


Figure 5. The interaction energies (kcal/mol) of the π -stacked $C_{16}H_{10}N_4$ dimers in the $C_{16}H_{10}N_4$ crystal (a) and in the cocrystal between $C_6F_4I_2$ and $C_{16}H_{10}N_4$ (b).

3.2. The Noncovalent Interactions in the Gas Phase

Under the same conditions, synthesis of the cocrystal between $C_6F_4I_2$ and $C_{16}H_{10}N_4$ succeeded, but syntheses of the cocrystal between $C_6F_4Br_2$ and $C_{16}H_{10}N_4$ and cocrystal between $C_6F_4Cl_2$ and $C_{16}H_{10}N_4$ failed. In order to uncover the underlying cause of the experimental discrepancies, we have investigated computationally the bifurcated halogen bonds between $C_6F_4X_2$ ($X = Cl, Br$ or I) and $C_{16}H_{10}N_4$ and the $\pi\cdots\pi$ stacking interactions between the $C_{16}H_{10}N_4$ molecules in the gas phase. The geometries of the dimer $C_{16}H_{10}N_4\cdots C_{16}H_{10}N_4$ and trimers $C_6F_4X_2\cdots(C_{16}H_{10}N_4)_2$ shown in Figure 6 were fully optimized at the PBE0-D3(BJ)/def2-TZVPP level of theory. Finally, it was found that all the optimized structures in Figure 6 have approximate C_2 symmetry. This means that the two bifurcated halogen bonds in each trimer are identical to each other. In fact, as can be seen in Figure 4, the interaction energy difference between the two bifurcated iodine bonds is only 0.58 kcal/mol, and two bifurcated iodine bonds in the cocrystal structure are also almost the same.

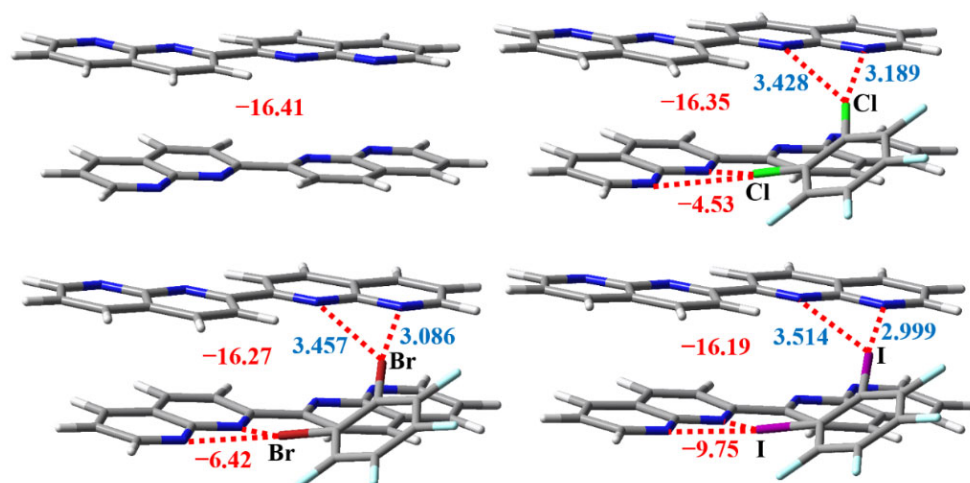


Figure 6. The PBE0-D3(BJ)/def2-TZVPP interatomic distances (blue numbers in Å) and interaction energies (red numbers in kcal/mol) for the complexes in the gas phase.

Figure 6 summarizes the $X\cdots N$ interatomic distances and interaction energies of the bifurcated halogen bonds and $\pi\cdots\pi$ stacking interactions in the four optimized complexes. The two $X\cdots N$ distances in each bifurcated halogen bond are obviously different, which shows that all the bifurcated halogen bonds are asymmetrical. The $I\cdots N$ distance of 2.999 Å is shorter than the $Br\cdots N$ distance of 3.086 Å and $Cl\cdots N$ distance of 3.189 Å, although the order of atomic radii is $I > Br > Cl$. Such an order of $X\cdots N$ interatomic distances reflects the strength order of the bifurcated halogen bonds, and indicates that the bifurcated iodine bond is much stronger than the bifurcated bromine bond and weakest bifurcated chlorine bond. There are two methods to calculate the interaction energies of the bifurcated halogen bonds and $\pi\cdots\pi$ stacking interactions in the three trimers in Figure 6. One method is to consider the mutual effects of the bifurcated halogen bonds and the $\pi\cdots\pi$ stacking interactions in the trimers, and the other method is not to consider these mutual effects. The interaction energies of the π -stacked $C_{16}H_{10}N_4$ dimers in $C_6F_4Cl_2\cdots(C_{16}H_{10}N_4)_2$, $C_6F_4Br_2\cdots(C_{16}H_{10}N_4)_2$ and $C_6F_4I_2\cdots(C_{16}H_{10}N_4)_2$ are -16.35 , -16.27 and -16.19 kcal/mol, respectively, without considering the effects of adjacent bifurcated halogen bonds. If we consider the effects of adjacent two bifurcated halogen bonds, the interaction energy of the π -stacked $C_{16}H_{10}N_4$ dimer can be calculated as the difference between the total interaction energy of the trimer and the total interaction energy of two identical bifurcated halogen bonds. Note that, as shown in Figure 6, the total interaction energy of two identical bifurcated halogen bonds in each trimer can be easily obtained if we treat the π -stacked $C_{16}H_{10}N_4$ dimer as one entity. Employing such a computational method, the interaction energies of the π -stacked $C_{16}H_{10}N_4$ dimers in $C_6F_4Cl_2\cdots(C_{16}H_{10}N_4)_2$, $C_6F_4Br_2\cdots(C_{16}H_{10}N_4)_2$ and $C_6F_4I_2\cdots(C_{16}H_{10}N_4)_2$ are calculated to be -16.32 , -16.24 and -16.16 kcal/mol, respectively. The differences between the interaction energies calculated from two different methods are quite small, which means that the mutual effects of the bifurcated halogen bonds and the $\pi\cdots\pi$ stacking interactions in the trimers can be neglected.

The interaction energy of the π -stacked $C_{16}H_{10}N_4$ dimer in the gas phase is -16.41 kcal/mol (Figure 6). Upon the trimer formation, it slightly decreases to -16.35 , -16.27 and -16.19 kcal/mol, respectively. In the cocrystal structure, the interaction energy of the π -stacked $C_{16}H_{10}N_4$ dimer is -16.47 kcal/mol (Figure 4). These similar values of interaction energy support that the $\pi\cdots\pi$ stacking interactions between the $C_{16}H_{10}N_4$ molecules are strong enough to be kept rigid in the solid and gas phases. The interaction energies of the bifurcated chlorine bond, bifurcated bromine bond and bifurcated iodine bond are -4.53 , -6.42 and -9.75 kcal/mol, respectively. This strength order is consistent with the one predicted by the $X\cdots N$ interatomic distances. The interaction energy of the bifurcated iodine bond in the gas phase is also close to the corresponding ones shown in Figure 4. The

binding energies of the monocentric C–I⋯N iodine bonds are less than 7.00 kcal/mol [42]. In contrast to the C–I⋯N monocentric iodine bonds, the C–I⋯(N,N) bifurcated iodine bonds are much stronger and much more rigid.

One C₁₆H₁₀N₄ molecule can form two bifurcated halogen bonds with two C₆F₄X₂ molecules. To explain why the C₁₆H₁₀N₄ crystal not the expected cocrystal between C₆F₄Cl₂ and C₁₆H₁₀N₄ or the expected cocrystal between C₆F₄Br₂ and C₁₆H₁₀N₄ was formed in the synthesis experiments, it is significant to compare the interaction energy of the π -stacked C₁₆H₁₀N₄ dimer in the C₁₆H₁₀N₄ crystal with the sum of the interaction energies of the two identical bifurcated halogen bonds. As can be seen in Figure 6, the values of the sum of the two interaction energies are −9.06, −12.84 and −19.50 kcal/mol for the bifurcated chlorine bond, bifurcated bromine bond and bifurcated iodine bond, respectively. Figure 5 shows that the interaction energy of the π -stacked C₁₆H₁₀N₄ dimer in the C₁₆H₁₀N₄ crystal is 11.22 kcal/mol. From the energetic point of view, only two bifurcated iodine bonds are strong enough to prevent the formation of the C₁₆H₁₀N₄ crystal. This explains why only the cocrystal between C₆F₄I₂ and C₁₆H₁₀N₄ was obtained in the synthesis experiments.

4. Conclusions

The unique enantiomeric pairs of double helices in the structure of the cocrystal between C₆F₄I₂ and C₁₆H₁₀N₄ have been reported in the present study. It was found that the formation of the cocrystal is driven by the strong bifurcated iodine bonds because they change the eclipsed arrangement of the π -stacked C₁₆H₁₀N₄ dimer in the C₁₆H₁₀N₄ crystal into the opposed arrangement in the cocrystal between C₆F₄I₂ and C₁₆H₁₀N₄. The C–I⋯(N,N) bifurcated iodine bond is much stronger than the C–I⋯N monocentric iodine bond. On the other hand, the strength of the C–I⋯(N,N) bifurcated iodine bond is not dependent on the N⋯N interatomic distance in the iodine atom acceptor.

In contrast to the cocrystal between C₆F₄I₂ and C₁₆H₁₀N₄, the cocrystal between C₆F₄Br₂ and C₁₆H₁₀N₄ and the cocrystal between C₆F₄Cl₂ and C₁₆H₁₀N₄ are difficult to be synthesized under the same conditions. To explain the underlying reasons for these differences, the interaction energies of the bifurcated halogen bonds and π ⋯ π stacking interactions in the gas phase have been calculated at the PBE0-D3(BJ)/def2-TZVPP level of theory. The absolute values of the interaction energies for the opposed configurations of the π -stacked C₁₆H₁₀N₄ dimers are all larger than 16.00 kcal/mol, which makes these π -stacked C₁₆H₁₀N₄ dimers hard to be affected by the adjacent bifurcated halogen bonds including the strongest bifurcated iodine bond with an interaction energy of −9.75 kcal/mol. The interaction energies of the bifurcated chlorine bond and bifurcated bromine bond are −4.53 and −6.42 kcal/mol, respectively. It is the much stronger bifurcated iodine bond that makes the cocrystal of C₆F₄I₂ and C₁₆H₁₀N₄ much easier to be synthesized.

In this study, the results clearly show that the stacking pattern of large aromatic molecules containing the N atoms can be changed by the halogen bond. Such a strategy may be useful in the design and synthesis of the organic optoelectronic materials.

Supplementary Materials: The following is available online at <https://www.mdpi.com/article/10.3390/cryst12070937/s1>, cif file of the cocrystal 2168308.

Funding: This research received no external funding.

Institutional Review Board Statement: Not applicable.

Informed Consent Statement: Not applicable.

Data Availability Statement: Data is contained within the article.

Acknowledgments: Z.W. acknowledges Luoyang Normal University for the chance to carry out the experiments during the outbreak of COVID-19 in 2020, and thanks the anonymous reviewers for their helpful comments and suggestions.

Conflicts of Interest: The author declares no conflict of interest.

References

1. Cavallo, G.; Metrangolo, P.; Milani, R.; Pilati, T.; Priimagi, A.; Resnati, G.; Terraneo, G. The Halogen Bond. *Chem. Rev.* **2016**, *116*, 2478–2601. [[CrossRef](#)] [[PubMed](#)]
2. Wang, H.; Wang, W.; Jin, W.J. σ -Hole Bond vs π -Hole Bond: A Comparison Based on Halogen Bond. *Chem. Rev.* **2016**, *116*, 5072–5104. [[CrossRef](#)] [[PubMed](#)]
3. Wang, W.; Zhang, Y.; Jin, W.J. Halogen Bonding in Room-Temperature Phosphorescent Materials. *Coord. Chem. Rev.* **2020**, *404*, 213107. [[CrossRef](#)]
4. Alkorta, I.; Elguero, J.; Frontera, A. Not Only Hydrogen Bonds: Other Noncovalent Interactions. *Crystals* **2020**, *10*, 180. [[CrossRef](#)]
5. Clark, T.; Hennemann, M.; Murray, J.S.; Politzer, P. Halogen Bonding: The σ -Hole. *J. Mol. Model.* **2007**, *13*, 291–296. [[CrossRef](#)]
6. Bulatova, M.; Ivanov, D.M.; Haukka, M. Classics Meet Classics: Theoretical and Experimental Studies of Halogen Bonding in Adducts of Platinum(II) 1,5-Cyclooctadiene Halide Complexes with Diiodine, Iodoform, and 1,4-Diiodotetrafluorobenzene. *Cryst. Growth Des.* **2021**, *21*, 974–987. [[CrossRef](#)]
7. Rajakumar, K.; Sharutin, V.V.; Adonin, S.A.; Zherebtsov, D.A.; Sakhapov, I.F.; Islamov, D.R.; Prabunatan, P.; Vershinin, M.A.; Naifert, S.A.; Polozov, M.A. Di- and Tetraiodoxylenes: Structure and Features of Non-Covalent Interaction in a Solid State. *J. Struct. Chem.* **2022**, *63*, 620–625. [[CrossRef](#)]
8. Kryukova, M.A.; Sapegin, A.V.; Novikov, A.S.; Krasavin, M.; Ivanov, D.M. New Crystal Forms for Biologically Active Compounds. Part 2: Anastrozole as N-Substituted 1,2,4-Triazole in Halogen Bonding and Lp - π Interactions with 1,4-Diiodotetrafluorobenzene. *Crystals* **2020**, *10*, 371. [[CrossRef](#)]
9. Eliseeva, A.A.; Ivanov, D.M.; Novikov, A.S.; Kukushkin, V.Y. Recognition of the π -Hole Donor Ability of Iodopentafluorobenzene—a Conventional σ -Hole Donor for Crystal Engineering Involving Halogen Bonding. *CrystEngComm* **2019**, *21*, 616–628. [[CrossRef](#)]
10. Ragusa, A.C.; Peloquin, A.J.; McMillen, C.D.; Pennington, W.T. 2,5-Diiodothiophene: A Versatile Halogen Bonding Synthron for Crystal Engineering. *Cryst. Growth Des.* **2022**, *22*, 1906–1913. [[CrossRef](#)]
11. Bondarenko, M.A.; Abramov, P.A.; Novikov, A.S.; Sokolov, M.N.; Adonin, S.A. Cu(II) Pentaiodobenzoate Complexes: “Super Heavy Carboxylates” Featuring Strong Halogen Bonding. *Polyhedron* **2022**, *214*, 115644. [[CrossRef](#)]
12. Posavec, L.; Nemec, V.; Stilinović, V.; Cinčić, D. Halogen and Hydrogen Bond Motifs in Ionic Cocrystals Derived from 3-Halopyridinium Halogenides and Perfluorinated Iodobenzenes. *Cryst. Growth Des.* **2021**, *21*, 6044–6050. [[CrossRef](#)] [[PubMed](#)]
13. Zheng, S.; Han, J.; Jin, X.; Ye, Q.; Zhou, J.; Duan, P.; Liu, M. Halogen Bonded Chiral Emitters: Generation of Chiral Fractal Architecture with Amplified Circularly Polarized Luminescence. *Angew. Chem. Int. Ed.* **2021**, *60*, 22711–22716. [[CrossRef](#)] [[PubMed](#)]
14. Scheiner, S. Comparison of Bifurcated Halogen with Hydrogen Bonds. *Molecules* **2021**, *26*, 350. [[CrossRef](#)]
15. Cinčić, D.; Friščić, T.; Jones, W. Experimental and Database Studies of Three-Centered Halogen Bonds with Bifurcated Acceptors Present in Molecular Crystals, Cocrystals and Salts. *CrystEngComm* **2011**, *13*, 3224–3231. [[CrossRef](#)]
16. Aakeröy, C.B.; Wijethunga, T.K.; Desper, J. Constructing Molecular Polygons Using Halogen Bonding and Bifurcated N-Oxides. *CrystEngComm* **2014**, *16*, 28–31. [[CrossRef](#)]
17. Efimenko, Z.M.; Eliseeva, A.A.; Ivanov, D.M.; Galmés, B.; Frontera, A.; Bokach, N.A.; Kukushkin, V.Y. Bifurcated μ_2 -I \cdots (N,O) Halogen Bonding: The Case of (Nitrosoguanidinate)Ni^{II} Cocrystals with Iodine(I)-Based σ -Hole Donors. *Cryst. Growth Des.* **2021**, *21*, 588–596. [[CrossRef](#)]
18. Gao, Y.J.; Li, C.; Liu, R.; Jin, W.J. Phosphorescence of Several Cocrystals Assembled by Diiodotetrafluorobenzene and Three Ring Angular Diazaphenanthrenes via C–I \cdots N Halogen Bond. *Spectrochim. Acta Part A* **2017**, *173*, 792–799. [[CrossRef](#)]
19. Sadhukhan, N.; Saha, S.; Bera, J.K. Multinuclear Complexes Derived from Bi-1, 8-naphthyridine Ligands. *J. Indian Chem. Soc.* **2015**, *92*, 1957–1964.
20. Cavallo, G.; Metrangolo, P.; Pilati, T.; Resnati, G.; Terraneo, G. Naming Interactions from the Electrophilic Site. *Cryst. Growth Des.* **2014**, *14*, 2697–2702. [[CrossRef](#)]
21. Politzer, P.; Murray, J.S.; Clark, T. Halogen Bonding: An Electrostatically-Driven Highly Directional Noncovalent Interaction. *Phys. Chem. Chem. Phys.* **2010**, *12*, 7748–7757. [[CrossRef](#)] [[PubMed](#)]
22. *CrysAlisPro, Rigaku Oxford Diffraction*, version 1.171.39.46; Oxford Diffraction Ltd.: Yarnton, UK, 2018.
23. Sheldrick, G.M. SHELXT—Integrated Space-Group and Crystal-Structure Determination. *Acta Crystallogr. Sect. A* **2015**, *71*, 3–8. [[CrossRef](#)] [[PubMed](#)]
24. Sheldrick, G.M. Crystal Structure Refinement with SHELXL. *Acta Crystallogr. Sect. C* **2015**, *71*, 3–8. [[CrossRef](#)]
25. Dolomanov, O.V.; Bourhis, L.J.; Gildea, R.J.; Howard, J.A.K.; Puschmann, H. OLEX2: A Complete Structure Solution, Refinement and Analysis Program. *J. Appl. Cryst.* **2009**, *42*, 339–341. [[CrossRef](#)]
26. Adamo, C.; Barone, V. Toward Reliable Density Functional Methods without Adjustable Parameters: The PBE0 Model. *J. Chem. Phys.* **1999**, *110*, 6158–6169. [[CrossRef](#)]
27. Grimme, S.; Antony, J.; Ehrlich, S.; Krieg, H. A Consistent and Accurate Ab Initio Parametrization of Density Functional Dispersion Correction (DFT-D) for the 94 Elements H–Pu. *J. Chem. Phys.* **2010**, *132*, 154104. [[CrossRef](#)] [[PubMed](#)]
28. Grimme, S.; Ehrlich, S.; Goerigk, L. Effect of the Damping Function in Dispersion Corrected Density Functional Theory. *J. Comput. Chem.* **2011**, *32*, 1456–1465. [[CrossRef](#)]
29. Weigend, F.; Ahlrichs, R. Balanced Basis Sets of Split Valence, Triple Zeta Valence and Quadruple Zeta Valence Quality for H to Rn: Design and Assessment of Accuracy. *Phys. Chem. Chem. Phys.* **2005**, *7*, 3297–3305. [[CrossRef](#)]

30. Boys, S.F.; Bernardi, F. The Calculation of Small Molecular Interactions by the Difference of Separate Total Energies. Some Procedures with Reduced Errors. *Mol. Phys.* **1970**, *19*, 553–566. [[CrossRef](#)]
31. Wang, W.; Sun, T.; Zhang, Y.; Wang, Y.B. The Benzene...Naphthalene Complex: A more Challenging System than the Benzene Dimer for newly Developed Computational Methods. *J. Chem. Phys.* **2015**, *143*, 114312. [[CrossRef](#)]
32. Wang, W.; Zhang, Y.; Wang, Y.B. Highly Accurate Benchmark Calculations of the Interaction Energies in the Complexes $C_6H_6 \cdots C_6X_6$ ($X = F, Cl, Br, \text{ and } I$). *Int. J. Quantum Chem.* **2017**, *117*, e25345. [[CrossRef](#)]
33. Frisch, M.J.; Trucks, G.W.; Schlegel, H.B.; Scuseria, G.E.; Robb, M.A.; Cheeseman, J.R.; Scalmani, G.; Barone, V.; Mennucci, B.; Petersson, G.A.; et al. *Gaussian 09, revision C.01*; Gaussian, Inc.: Wallingford, CT, USA, 2010.
34. Ng, C.-F.; Chow, H.-F.; Mak, T.C.W. Halogen-Bond-Mediated Assembly of a Single-Component Supramolecular Triangle and an Enantiomeric Pair of Double Helices from 2-(Iodoethynyl)pyridine Derivatives. *Angew. Chem. Int. Ed.* **2018**, *57*, 4986–4990. [[CrossRef](#)] [[PubMed](#)]
35. Liu, C.-Z.; Koppireddi, S.; Wang, H.; Zhang, D.-W.; Li, Z.-T. Halogen Bonding Directed Supramolecular Quadruple and Double Helices from Hydrogen-Bonded Arylamide Foldamers. *Angew. Chem. Int. Ed.* **2019**, *58*, 226–230. [[CrossRef](#)] [[PubMed](#)]
36. Koppireddi, S.; Liu, C.-Z.; Wang, H.; Zhang, D.-W.; Li, Z.-T. Halogen and Hydrogen Bonding-Driven Self-Assembly of Supramolecular Macrocycles and Double Helices from Hydrogen-Bonded Arylamide Foldamers. *CrystEngComm* **2019**, *21*, 2626–2630. [[CrossRef](#)]
37. Liu, C.-Z.; Koppireddi, S.; Wang, H.; Zhang, D.-W.; Li, Z.-T. Halogen Bonding-Driven Formation of Supramolecular Macrocycles and Double Helix. *Chin. Chem. Lett.* **2019**, *30*, 953–956. [[CrossRef](#)]
38. Xu, Y.; Hao, A.; Xing, P. $X \cdots X$ Halogen Bond-Induced Supramolecular Helices. *Angew. Chem. Int. Ed.* **2022**, *61*, e202113786.
39. Pitoňák, M.; Neogrady, P.; Řezáč, J.; Jurečka, P.; Urban, M.; Hobza, P. Benzene Dimer: High-Level Wave Function and Density Functional Theory Calculations. *J. Chem. Theory Comput.* **2008**, *4*, 1829–1834. [[CrossRef](#)]
40. Groom, C.R.; Bruno, I.J.; Lightfoot, M.P.; Ward, S.C. The Cambridge Structural Database. *Acta Crystallogr. Sect. B* **2016**, *72*, 171–179. [[CrossRef](#)] [[PubMed](#)]
41. Gierschner, J.; Lüer, L.; Milián-Medina, B.; Oelkrug, D.; Egelhaaf, H.-J. Highly Emissive H-Aggregates or Aggregation-Induced Emission Quenching? The Photophysics of All-Trans para-Distyrylbenzene. *J. Phys. Chem. Lett.* **2013**, *4*, 2686–2697. [[CrossRef](#)]
42. Wang, W.; Zhang, Y.; Wang, Y.-B. The $\pi \cdots \pi$ Stacking Interactions between Homogeneous Dimers of $C_6F_xI_{(6-x)}$ ($x = 0, 1, 2, 3, 4, \text{ and } 5$): A Comparative Study with the Halogen Bond. *J. Phys. Chem. A* **2012**, *116*, 12486–12491. [[CrossRef](#)]